Impact of Contacting Geometries When Measuring Fill Factors of Solar Cell Current–Voltage Characteristics

Christian N. Kruse, Martin Wolf, Carsten Schinke, David Hinken, Rolf Brendel, and Karsten Bothe

***Abstract*—We analyze the influence of a variety of different contacting geometries on the fill factor (FF) of solar cell *I–V* measurements. For this analysis, we compare a wide variety of modeled and measured FFs of Si solar cells. We consistently find large FF differences between individual contacting geometries. These differences amount to up to $3\%_{\mathrm{abs}}$ for high busbar resistivities of up to $40\,\Omega/\mathrm{m}$. We analyze the contacting geometries for their sensitivity on uncontrolled variations of the contacting resistances. In this analysis, we find that using triplet rather than tandem configurations and using a larger number of test probes reduces the impact of varying contacting resistances to below $0.02\%_{\mathrm{abs}}$. We propose a contacting geometry that we consider to be suitable for calibrated *I–V* measurements. This contacting scheme is a configuration with a total of five triplets consisting of two current probes and one sense probe. The sense probe is positioned to measure the average busbar potential between the current probes. This is the optimal contacting geometry in terms of a low sensitivity to the busbar resistivity and variations of contacting resistances. In addition, this geometry does not impose unnecessarily large mechanical stress to the cell under measurement.**

***Index Terms*—Characterization of photovoltaics (PV), current–voltage characteristics, IEC standards.**

I. Introduction

CONTACTING of bare silicon solar cells is a challenging task in solar cell calibration measurements. In order to maintain comparability between laboratories and industrial partners worldwide, a number of measurement conditions have been standardized (IEC 60751, IEC 60891, and IEC 60904). Unfortunately, many aspects of the contacting of bare cells have yet to be covered by any of the international standards. Even though a number of different contacting issues such as the number of contacting pins [1], misalignment of contacting bars [1], [2], as well as asymmetric current collection [3] have already been discussed, the correct way of contacting bare solar cells is still under debate.

While some authors [4], [5] demand a contacting, which reflects the module integration, others [3], [6] recommend a contacting scheme that represents a perfectly conducting busbar (BB). Regardless of which of these approaches will finally be taken into consideration in a standardization process, current–voltage (*I–V*) testers in research and industry currently use many different contacting schemes. This raises the following question: What deviations in the characteristic solar cell parameters do these different schemes imply? This paper, therefore, analyzes the impact of contacting schemes on the measured fill factors (FFs).

Testing solar cells with front and rear contacts requires contacting the cell's front side while keeping the shading of the cell to a minimum. Using narrow contacting bars equipped with spring-loaded probes to contact the front-side BBs in a four-wire configuration is the most common approach. It is realized with varying numbers of current and sense probes and various positionings along the BBs.

We investigate the impact of a variety of different contacting geometries on the FF of solar cell *I–V* curves by means of analytical and numerical modeling and confirm the modeling by measurements. As a result, we propose a contacting scheme suitable for calibrated *I–V* measurements at the Calibration and Test Center at the Institute for Solar Energy Research Hamelin (ISFH CalTeC) that is DAkks accredited according to the IEC 60904 standards.

II. Approach

In order to study the impact of the contacting scheme on the FF of solar cell *I–V* measurements, we perform analytical and numerical modeling. The modeling results of eight different contacting schemes are tested by means of solar cell *I–V* measurements using a freely configurable contacting bar. After finding consistency between modeling and measurement, we run an optimization approach to identify an optimal contacting layout suitable for calibrated *I–V* measurements. Our optimization approach is based on probing the average BB potential of the cell, assuming that the average BB potential is a good approximation for the solar cells operating voltage. We model the impact of the BB conductivity, as well as the sensitivity of the different

Manuscript received January 12, 2017; revised February 22, 2017; accepted February 27, 2017. This work was part of the European Metrology Research Programme (EMRP). The EMRP is jointly founded by the EMRP participating countries within EURAMET and the European Union.

C. N. Kruse, M. Wolf, D. Hinken, and K. Bothe are with the Institute for Solar Energy Research Hamelin, Emmerthal 31860, Germany (e-mail: c.kruse@isfh.de; wolf@isfh.de; d.hinken@isfh.de; k.bothe@isfh.de).

C. Schinke and R. Brendel are with the Institute for Solid State Physics, Leibniz Universität Hannover, 30167 Hannover, Germany, and also with the Institute for Solar Energy Research Hamelin, Emmerthal 31860, Germany (e-mail: c.schinke@isfh.de; r.brendel@isfh.de).

Color versions of one or more of the figures in this paper are available online at http://ieeexplore.ieee.org.

Digital Object Identifier 10.1109/JPHOTOV.2017.2677084

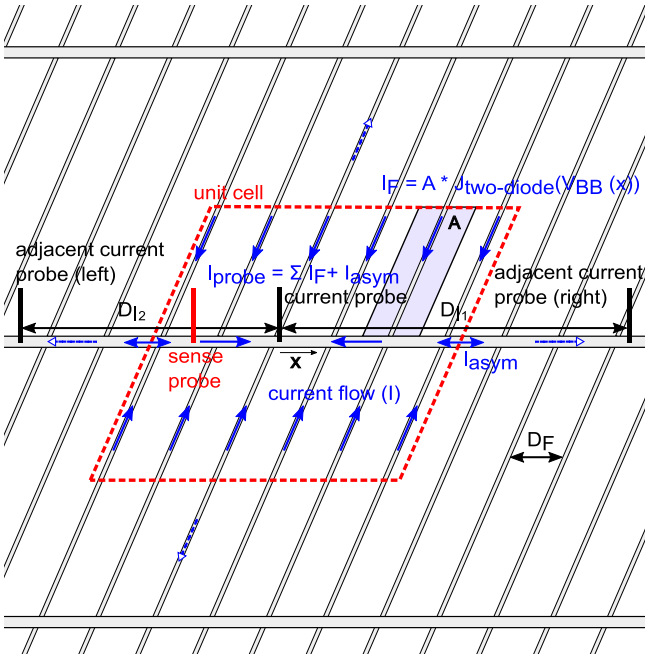

Fig. 1. Analytical model: The gray grid represents the front metallization of a solar cell. The current flow (blue arrows) is axis symmetric with respect to the BBs and with respect to the current probes (black bars) except for a small contribution I_{asym}. In general, the left and right adjacent contacting probes are at different distances to the center current probe. For the current through the center current probe, the current from the fingers within the unit cell (red-dashed line) and I_{asym} are considered. Each finger delivers the current of a subcell with area A (shaded area). For the *I–V* characteristic, the voltage is calculated at the position of the sense probe (red bar).

contacting layouts to variations of the contacting resistance of individual test probes. The advantage of analytical modeling is the speed of the calculation. This allows us to study a larger number of different contacting schemes and BB conductivities and thus accelerates the optimization approach considerably. The use of the numerical device simulation program Griddler [7] allows for taking probe-to-probe variations of the contacting resistances into account. These variations cause asymmetric potential distributions along the BB that are difficult to treat analytically.

A. Analytical Model

The model assumes the following:

1) The solar cell is composed of an array of sub solar cells, with the *I–V* characteristic of these subcells being described by the two-diode model [8]. All subcells have identical parameters.
2) No direct current flowing from the semiconductor into the BB is considered. All current in the BB is provided via the cell fingers.
3) The current flows are symmetric with respect to the current probes and the BBs and
4) The sense probes do not influence the BB potential (no current for sensing).

A schematic of the analytical model is shown in Fig. 1.

Following these assumptions, we get the current flow through each current probe:

$$I_{\mathrm{probe}} = \sum_{n=1}^{\lfloor \frac{D_{\mathrm{I}_1}}{2D_{\mathrm{F}}} \rfloor} I_{F,n}(V_n) + \sum_{n=1}^{\lfloor \frac{D_{\mathrm{I}_2}}{2D_{\mathrm{F}}} \rfloor} I_{F,n}(V_n) + I_{\mathrm{asym}}(V_{\mathrm{edge}}) \tag{1}$$

where $D_{\mathrm{I}_{1,2}}$ are the distances between one current probe and its two adjacent current probes, D_{F} is the distance between adjacent fingers, $I_{F,n}$ is the current flow from the finger n, and V_n is the BB potential at finger n. The symbols $\lfloor\rfloor$ and $\lceil\rceil$ round down and up to the nearest integer, respectively.

For an arbitrary position of the current probes relative to the metal grid, the unit cell boundary is not necessarily located in the center between two fingers. As current from inside the unit cell can be collected by a finger outside the unit cell, this current has to be accounted for by a current I_{asym} in the BB through the unit cell edge. This ensures an independence of the current probe positioning relative to the metal grid.

The current from each finger is calculated using the two-diode equation. However, this current depends on the BB potential at the finger position, which, in turn, depends on the current through the BB and, hence, the current from each finger. This makes a closed solution of the problem impossible. Therefore, we use an iterative approach to solve (1). We first calculate the voltage potential along the BB:

$$\begin{aligned} V_{x,i+1} = & \sum_{m=1}^{\lfloor \frac{x}{D_{\mathrm{F}}} \rfloor} R_{\mathrm{BB}} \cdot m \cdot D_{\mathrm{F}} \cdot I_{F,m}(V_{m,i}) \\ & + \sum_{m=\lceil \frac{x}{D_{\mathrm{F}}} \rceil}^{\lfloor \frac{D_{\mathrm{I}}}{2D_{\mathrm{F}}} \rfloor} R_{\mathrm{BB}} \cdot x \cdot I_{F,m}(V_{m,i}) \\ & + R_{\mathrm{BB}} \cdot x \cdot I_{\mathrm{asym}}(V_{\mathrm{edge}}) \end{aligned} \tag{2}$$

where i is the ith number of iteration, x is the distance to the current probe, and R_{BB} is the BB line resistance. Equation (2) is then repeatedly applied until a threshold $|V_{x,i+1} - V_{x,i}| \leq V_{\mathrm{thres}} = 0.001$ mV is reached for all $0 \leq x \leq \frac{D_{\mathrm{I}}}{2}$. To simulate an entire *I–V* curve for a contacting layout, we take several starting voltages $V_{0,0}$ and then calculate the voltage potential at the sense probe position and the voltage distribution with (2) and the total current with (1) using the voltage distribution.

Using this model, we calculate BB potentials and entire *I–V* characteristics on short time scales, allowing us to analyze a large number of contacting layouts for various different BB conductivities.

B. Numerical Modeling

As our analytical model takes advantage of the symmetry of the contacting layouts, it is not suitable to analyze effects on cell level. Such effects can, for example, be inhomogeneous contacting resistances or edge effects. Therefore, we also use the numerical solar cell simulator Griddler [7]. Griddler is a

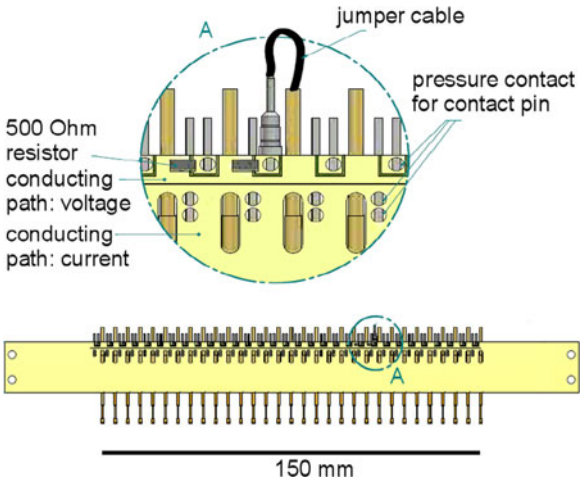

Fig. 2. Design of the freely configurable contacting bar (pv-tools [10]). Each of the 31 removable contacting probes is connected to a jumper cable using a pressure contact. Each jumper cable can be connected to either the voltage conducting path using a 500 Ω resistor or to the current conducting path.

simulation tool for optimizing the front metallization pattern of solar cells. However, it can also be used to simulate the *I–V* characteristics of a solar cell for different contacting layouts. In particular, Griddler can analyze the impact of resistance deviations of individual contacting current probes on the *I–V* curve of the solar cell.

C. Experimental Setup

To verify our modeling results experimentally, we measure *I–V* curves of a solar cell with different contacting layouts. All measurements are performed on a five-BB passivated emitter and rear totally diffused (PERT) solar cell manufactured at ISFH. The front-side metallization of the cell was screen printed in two separate steps for the BBs and the fingers using a silver paste. For this front-side metallization, featuring 0.5-mm-wide BBs, we measure a BB resistance of $R_{\mathrm{BB}} = 34\ \Omega/\mathrm{m}$ using a four-wire setup. The BB resistivities of conventional front-side metallizations of industrial five-BB solar cells are, from our experience, usually below $R_{\mathrm{BB}} = 40\ \Omega/\mathrm{m}$. The high but still realistic BB resistance is the reason why we choose this cell, because the impact of contacting schemes on the *I–V* characteristic will increase with a higher BB resistance. Further details of the solar cell can be found in [9].

To perform the measurement for many contacting geometries efficiently, we use a contacting bar (pv-tools [10]) with a 5-mm distance between the removable test probes, where each probe can either be a current or a sense probe (see Fig. 2). In this freely configurable contacting bar, each of the up to 31 test probes is connected to a jumper cable by a pressure contact. This jumper cable can be connected to either the voltage conduction path over a 500 Ω resistor or to the current conduction path. Thus, each test probe can be a sense or a current probe. As the resistance of the current conduction path is negligible, all current probes are on the same potential. This enables us to measure different contacting layouts with one set of contacting bars.

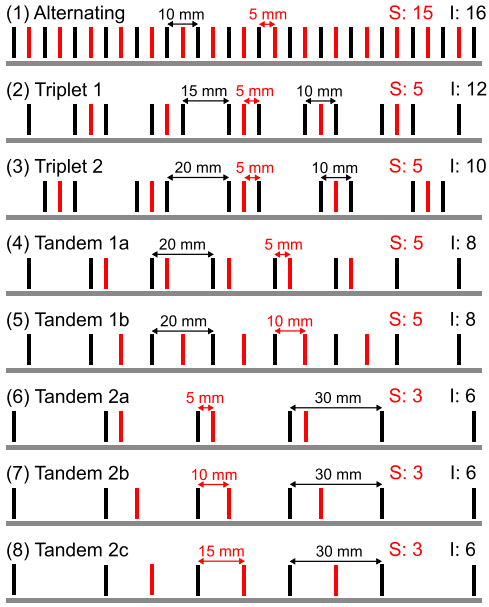

Fig. 3. Contacting geometries realized with the freely configurable contacting bar for the comparison of the different approaches. Black bars represent the current probes and red bars the sense probes.

Based on this contacting bar, we define eight layouts (see Fig. 3) to compare the modeling results and the measurements for a variety of contacting configurations.

III. Modeling Results

Using our analytical model, we calculate the BB potential between adjacent current probes. The sets of input parameters for analytical and numerical modeling were independently chosen to reproduce the experimentally determined short-circuit current, open-circuit voltage, and FF of our five-BB PERT cell (see Section II-C) and can be found in the Appendix. All analyses in this work are performed for five-BB solar cells with differing BB resistances. The concept presented in this work is, however, also suitable for cells with a different number of BBs, provided the current collected by each BB is adjusted to the distance between the BBs. For tandem and triplet configurations, we calculate the BB potential from the current probe to one or two adjacent current probes, respectively. An example of calculated BB potentials is shown in Fig. 4(a) for contacting layout Tandem 2 for several voltages applied to the current probe. The vertical lines mark the sense positions of the Tandem 2a–2c configurations; the current probes are at $x = 0$ mm and $x = 30$ mm. In Fig. 4(b), the *I–V* characteristics for the corresponding sense positions are shown. The dashed lines show the results from numerical modeling. As the sets of input parameters for analytical and numerical modeling were independently chosen to reproduce the measured *I–V* characteristics of the solar cell, the shapes of the resulting *I–V* curves differ slightly from each other.

The open-circuit voltage does not depend on the contacting scheme, because there is no current flowing through the BB. As

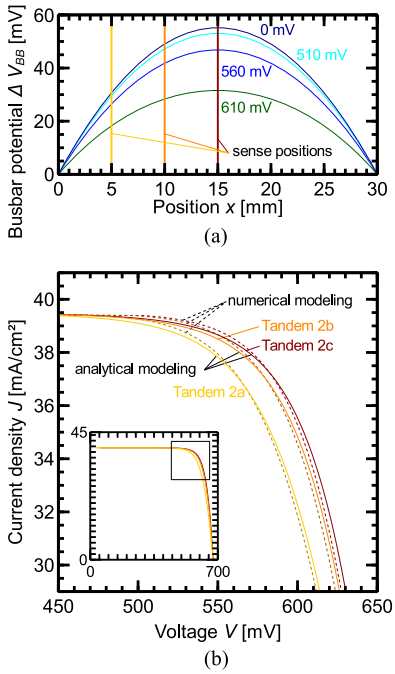

Fig. 4. Modeled BB potential and *I–V* characteristics for the Tandem 2 configurations. The BB potential to one adjacent current probe is calculated for four different voltages applied to the current probe using the analytical model. The current probes are located at 0 and 30 mm. The sense probes are located corresponding to the vertical lines in (a). The *I–V* characteristics are modeled with the analytical model (solid lines) and the numerical simulation (dashed lines).

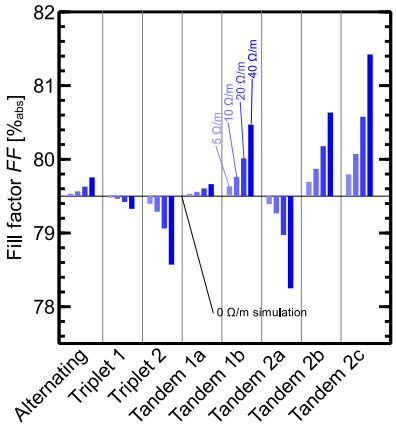

Fig. 5. Impact of the BB resistance on the FF for the contacting layouts 1–8 calculated with the analytical model. The blue bars show the FF deviation for four BB resistivities from the $R_{\mathrm{BB}} = 0\ \Omega/\mathrm{m}$ case, which yields the same result for each contacting geometry.

the *I–V* curve only has a very small gradient at low voltages, the short-circuit current is also independent of the contacting scheme, because a shift toward higher voltages, caused by the voltage drop along the BB, will result in almost the same current. The largest impact of the contacting geometry is at high currents and high voltages, at which the *I–V* curve has a steep gradient. This is at the maximum power point. Consequently, it is only the FF that shows a dependence on the contacting

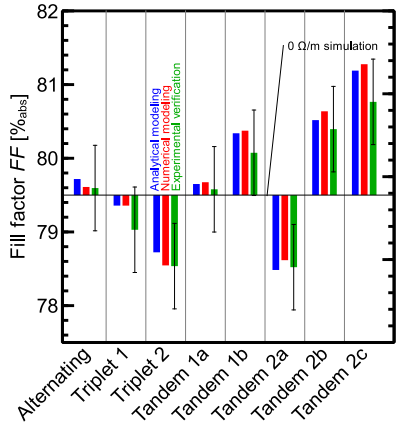

Fig. 6. Comparison of the results of the analytical and numerical modeling with the results of measurements using the freely configurable contacting bar. The agreement of the datasets shows the applicability of the modeling approaches determining the impact of the contacting layout on FF. The BB resistance of the analyzed cell is 34 Ω/m.

scheme. Therefore, we concentrate our following analysis on the FF of *I–V* characteristics.

Using our analytical model, we calculate the FF of our five-BB solar cell for the contacting layouts (1–8) displayed in Fig. 3. Keeping all other cell parameters constant, we now vary the BB line resistance between $R_{\mathrm{BB}} = 0\ \Omega/\mathrm{m}$ and $R_{\mathrm{BB}} = 40\ \Omega/\mathrm{m}$ corresponding to sheet resistances of up to 20 mΩ/sq. The results are shown in Fig. 5. For each contacting layout, the bars show FF deviations from the $R_{\mathrm{BB}} = 0\ \Omega/\mathrm{m}$ case, which yields the same result for all contacting layouts, for four BB resistances between $R_{\mathrm{BB}} = 5\ \Omega/\mathrm{m}$ and $R_{\mathrm{BB}} = 40\ \Omega/\mathrm{m}$. Our model shows more than $3\%_{\mathrm{abs}}$ deviations for the FF of the same cell for high BB resistances of $R_{\mathrm{BB}} = 40\ \Omega/\mathrm{m}$. This corresponds to a difference in the conversion efficiency of more than $0.8\%_{\mathrm{abs}}$. At $R_{\mathrm{BB}} = 20\ \Omega/\mathrm{m}$, the model shows $\Delta\mathrm{FF} = 1.6\%_{\mathrm{abs}}$ FF and $\Delta\eta = 0.4\ \%_{\mathrm{abs}}$ conversion efficiency differences. This calculation indicates the necessity of a careful design of the contacting geometries.

IV. Experimental Verification

To ensure the applicability of our modeling approaches, we compare modeling to measurements for geometries 1–8 in Fig. 3. Fig. 6 shows the results of this comparison.

Analytical (blue bars) and numerical (red bars) modeling yield very similar FFs, and both are in good agreement with the measured FFs (green bars). As shown in Fig. 4, slightly different *I–V* curves result from analytical and numerical modeling. This is due to the fact that numerical modeling takes the edges of the BB and the cell into account, which are neglected in the analytical model. Deviations between modeling and the experimental verification rise from the uncertainty of the measured FFs, which is in the order of $0.6\%_{\mathrm{abs}}$. Keeping in mind these uncertainties, Fig. 6 proofs the applicability of both analytical and numerical modeling for analyzing the influence of contacting geometries on the FF in *I–V* measurements.

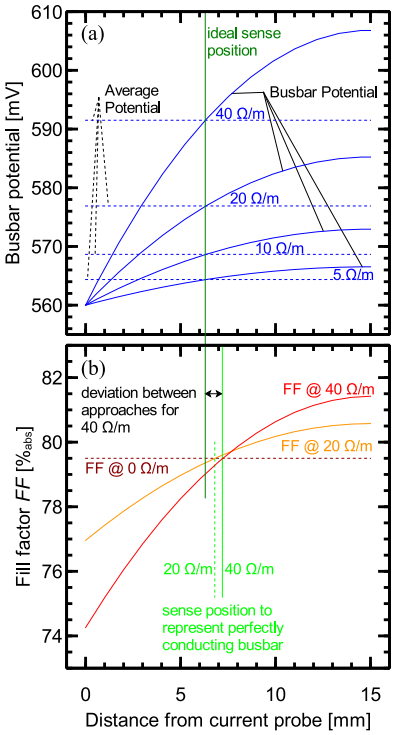

Fig. 7. (a) BB potentials (solid blue lines) and average BB potentials (dashed blue lines) for the Tandem 2 configuration. The dark green line marks the intersection of the potential distribution and the average potential and is the ideal sense position according to our recommendation. (b) FFs as a function of the distance between sense and current contact for $R_{\mathrm{BB}} = 40\ \Omega/\mathrm{m}$ (solid red line) and $R_{\mathrm{BB}} = 20\ \Omega/\mathrm{m}$ (solid orange line). The dashed red line shows the FF of a cell with a perfectly conducting BB. The light green lines mark the ideal sense position corresponding to the approach found in [6] of placing the sense probe to represent a perfectly conducting BB.

V. Optimization

We optimize the contacting geometry in terms of the current probe distance, the sense probe position, and the total number of test probes by experimentally verified modeling. As we aim for a comparability between different experimental setups, we suggest probing the average BB potential, which is an approximation for the operating voltage of the cell. This situation is shown for the Tandem 2 configuration in Fig. 7.

The solid blue lines in Fig. 7(a) show the BB potential at the maximum power point, while the dashed blue lines show the average BB potential (no dependence on position x) for different BB resistivities R_{BB}. The dark green line marks the intersection of the BB potential and the average potential. This position does not depend on the BB conductivity and is our suggestion for the ideal sense position. The solid red and orange lines in Fig. 7(b) show the FF when placing the sense probe at the different distances from the current probe for $R_{\mathrm{BB}} = 40\ \Omega/\mathrm{m}$ and $R_{\mathrm{BB}} = 20\ \Omega/\mathrm{m}$, respectively. The dashed red line shows the FF of a perfectly conducting BB. Another approach for the ideal sense position found in the literature [6] is to place the sense probe to represent a perfectly conducting BB at the intersection of the dashed red line and the solid red and orange lines (light green solid and dashed line). However, for a large current probe spacing, this position depends on the BB conductivity. It should

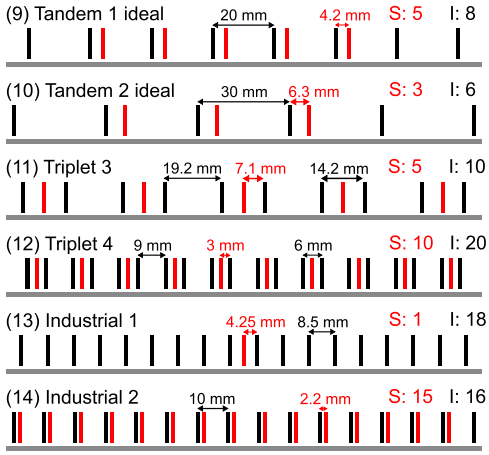

Fig. 8. Contacting schemes investigated for the determination of the optimal contacting geometry. Black bars represent the current probes and red bars the sense probes.

be noted that the contacting geometry in [6] features a small current probe spacing and, thus, minimizes this effect. For Tandem 2, this results in a 0.8-mm difference between the sense positions of both approaches for $R_{\mathrm{BB}} = 40\ \Omega/\mathrm{m}$ and a FF deviation of ca. $0.5\%_{\mathrm{abs}}$. However, with decreasing distance between the current probes, the difference between the approaches decreases significantly. For the Tandem 1 configuration (20-mm current probe spacing), the difference is only 0.2 mm. Both approaches would yield exactly the same result if the entire solar cell was in fact operated at the average BB potential. However, due to the large inhomogeneities in the cell potential, this assumption leads to an overestimation of the current and, thus, an overestimation of the FF. Consequently, the FF when sensing the average BB potential is slightly lower than the FF of a cell with a superconducting BB.

The overestimation of the current can be best explained with a gedanken experiment: In a theoretical cell, the BB potential is such that one half of the cell is at short-circuit, while the other half is at open-circuit conditions. Now, the average BB potential is half the open-circuit voltage, for which we would estimate a current still close to the short-circuit current due to the *I–V* characteristics of the cell. However, the actual current is half the short-circuit current rising from the half of the cell in short-circuit conditions, while the other half delivers no current. Thus, we overestimate the current by roughly 100%.

Of course, the overestimation in real measurements is a lot smaller but increases with larger distances of the current probes due to the larger inhomogeneity of the BB potential.

For ideal current probe spacing, both approaches yield the same sense probe position and, consequently, the same FF, which is the FF of a cell with a perfectly conducting BB. Therefore, we design our optimized contacting geometries to probe the average BB potential and evaluate the geometries by calculating the deviation of the FF to the FF of a cell with a perfectly conducting BB (intersection of dark green with red and orange lines in Fig. 7).

The optimized contacting geometries are shown in Fig. 8. Geometries 9 and 10 are optimized schemes rising from layout

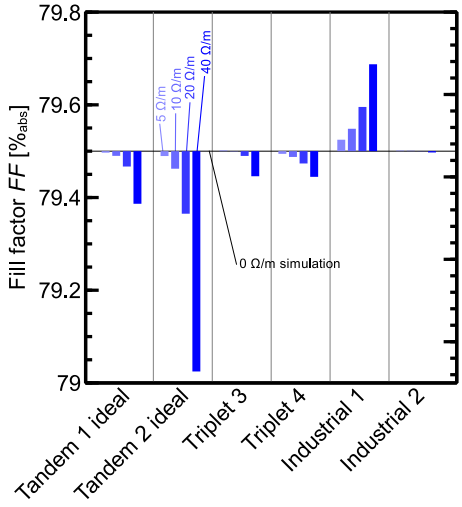

Fig. 9. Impact of the BB resistance on the FF for contacting layouts 9–14 calculated with the analytical model (different scale than Fig. 5). The blue bars show the FF deviation for four BB resistivities from the $R_{\mathrm{BB}} = 0\ \Omega/\mathrm{m}$ case, which yields the same result for each contacting geometry.

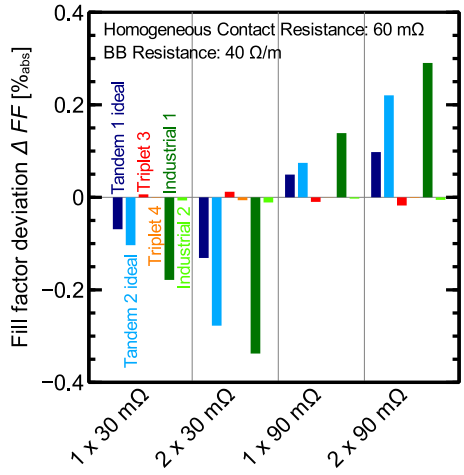

Fig. 10. Deviation in the FF as a function of the number and resistance of differently contacting current probes at positions adjacent to a sense probe. The results were obtained by numerical modeling.

Tandem 1 and Tandem 2, respectively. Geometry 11 is an optimization of the layouts Triplet 1 and Triplet 2. We also include one geometry found in [6] (Triplet 4) and two geometries used in industrial cell testers in our comparison.

We compare the optimized layouts for their sensitivity on the BB resistance and varying contacting resistances of the test probes.

A. *Sensitivity on the Busbar Conductivity*

We assume that the average BB potential is a good approximation for the cell potential. Consequently, the measurement results should be independent of the BB resistance. Using our analytical model, we calculate the FF as a function of the BB resistance for contacting layouts 9–14 (see Fig. 8). The results are shown in Fig. 9. The contacting schemes Triplet 3, Triplet 4, and Industrial 2 show only a small dependence of the calculated FFs on varying BB resistivity, due to the small potential variation along the BB. Using the Industrial 1 layout leads to higher FFs for increasing BB resistivity, because the sense probe is at a position of higher BB potential. Although both Tandem 1 ideal and Tandem 2 ideal are designed to probe the average BB potential, they still show a strong dependence of the FF on the BB resistivity. This rises from the large potential variation along the BB due to the large spacing of the current probes. Consequently, contacting schemes should feature an average contacting probe spacing of less than 20 mm.

B. *Sensitivity to Inhomogeneous Contacting Resistances*

In this section, we analyze the contacting layouts shown in Fig. 8 in terms of their sensitivity on variations of the contacting resistance of individual current probes.

We experimentally determine the contacting resistance of our nine-point crown test probes with a diameter of 1.15 mm to be $R_{\mathrm{C}} = (60 \pm 20)\ \mathrm{m}\Omega$ using a four-wire setup. The uncertainty is determined from reproducibility after recontacting, measuring at the same BB positions. It should be noted that the contacting resistance decreases for the first two to five times of contacting at the same position on the BB. Therefore, we contact the cell ten times at the same BB positions before we start our measurement.

To analyze the impact of these deviations on the FF measurement of our five-BB PERT cell, we use numerical modeling of the entire solar cell. We apply contacting resistances of $R_{\mathrm{C}} = 30\ \mathrm{m}\Omega$ or $R_{\mathrm{C}} = 90\ \mathrm{m}\Omega$ to one or two contacting probes per BB (x-axis of Fig. 10). For all contacting probes not specified on the x-axis of Fig. 10, we apply a contacting resistance of $R_{\mathrm{C}} = 60\ \mathrm{m}\Omega$. This is a worst case for the variation of the contacting resistances. As long as the current probes with deviating contacting resistance are adjacent to a sense probe, the impact on the FF is independent of the exact location of the contacting resistance variation. For a good comparability of the simulations, we ensure that all current probes with a deviating contacting resistance are located adjacent to a sense probe. The results are shown in Fig. 10 as deviations in $\%_{\mathrm{abs}}$ from the FF using a homogeneous contacting resistance. Both Tandem configurations (dark and light blue bars) and the Industrial 1 configuration (dark green bars) are much more sensitive to deviations in the contacting resistance than the Triplet configurations (red and orange bars) and the Industrial 2 configuration (light green bars). Following from the differences between the configurations Tandem 1, Tandem 2, Industrial 1, and Industrial 2, one factor determining the impact of varying contacting resistances is the total number of sense probes. While the Industrial 1 layout (1 sense probe) shows the largest dependence on varying contacting resistances, the dependence decreases with an increasing number of sense probes. The Industrial 2 layout (15 sense probes) shows nearly no impact of varying contacting resistances.

The number of sense probes is, however, not the only factor determining the impact of varying contacting resistances. Although the Triplet 3 and Tandem 1 configurations both feature five sense probes, the impact of varying contacting resistance is

TABLE I
COMPARISON OF THE OPTIMAL CONTACTING GEOMETRY (TRIPLET 3) TO A MEASUREMENT PERFORMED AT ISE CALLAB

Geometry	I_{sc} [A]	V_{oc} [mV]	FF [$\%_{abs}$]	U(FF) [$\%_{abs}$]
Triplet 3	9.44	674.7	79.73	0.59
ISE CalLab	9.44	673.8	79.49	0.52

about one order of magnitude smaller for the Triplet 3 configuration. Due to the close proximity of the sense probe to one current probe in tandem configurations, each change of the BB potential at the current probe is directly transferred to the sense probe. In triplet configurations, this effect is minimized by the equal distance of one sense probe to two current probes.

Consequently, a triplet configuration shows a better reproducibility than a tandem configuration featuring the same amount of sense probes.

C. Optimized Contacting Geometry

Due to the strong dependence of the FF on the BB conductivity and inhomogeneous contacting resistances for the contacting schemes Tandem 1 ideal, Tandem 2 ideal, and Industrial 1, these layouts are not suitable for the application in a calibration laboratory. This leaves the layouts Triplet 3, Triplet 4, and Industrial 2 as possible candidates for the optimal contacting layout. As Triplet 3 has about half the number of contacting probes compared with Triplet 4 and Industrial 2, the risk of damage due to mechanical stress applied to the cell is also about half when measuring with contacting layout Triplet 3. Thus, we choose contacting geometry Triplet 3 for measurements of the *I–V* characteristics in our calibration laboratory at ISFH CalTeC.

After fabricating a new set of contacting bars featuring the Triplet 3 layout, we measure the five-BB PERT cell from Section II-C with this set of contacting bars and compare the results with an independent measurement at ISE CalLab. The results are shown in Table I. The short-circuit current (I_{sc}) and the open-circuit voltage (V_{oc}) are also included in Table I and, taking into account the respective uncertainties, I_{sc} and V_{oc} are equal in both measurements. This ensures a good comparability of both FF measurement results. In order to compare both measurements, we calculate the equality E_n of the measured FFs and their respective uncertainties (U(FF)) according to [11]. Two measurements are considered equal if $|E_n| < 1$. This calculation yields $E_n = 0.31$ for our measurement and the one performed at ISE CalLab, and thus, both measurements are considered equal. Furthermore, the total uncertainty of the measurement, rising from various characteristics of the experimental setup, is about one order of magnitude larger than any uncertainty rising from the contacting of the solar cell, even for large BB resistivities of $R_{BB} = 40\ \Omega/\mathrm{m}$.

VI. CONCLUSION

We demonstrated the necessity of a careful design of contacting layouts, depending on the purpose of the measurement. If a comparability between different laboratories and cell testers is the aim, we suggest placing the sense probes at the position of the average BB potential. This is, for reasonably small distances between current probes and BB resistivities, equal to neglecting the BB resistance. We modeled different contacting layouts and analyzed their dependence on the BB resistance finding differences in the calculated FF of up to $3\%_{abs}$. Based on these modeling results, we designed three contacting layouts probing the average BB potential and analyzed these layouts, as well as one layout presented in [6] and two industrially used layouts for their sensitivity on the BB conductivity. We found that the current probe spacing should be below 20 mm to minimize the variation of the potential along the BB. Furthermore, we analyzed these contacting schemes for their sensitivity on inhomogeneous contacting resistances. In this analysis, we found that using a large number of sense probes as well as using triplet rather than tandem configurations reduces the impact of inhomogeneous contacting resistances on the FF of the measured *I–V* characteristic. For screen-printed five BB solar cells, we find that a geometry with five triplets per BB is enough to ensure a reasonable robustness to varying contacting resistances. As a reduction of the total number of contacting probes also reduces the risk of damage due to mechanical stress, we chose the layout for the solar cell calibration laboratory at ISFH CalTeC to be the Triplet 3 configuration presented in this paper.

TABLE II
INPUT PARAMETERS FOR THE TWO-DIODE MODEL USED FOR THE ANALYTICAL MODEL (SECTION II-A)

input parameter	input value
photo generated current J_{Ph}	$39.5\ \mathrm{mA/cm^2}$
saturation current density (diode 1) J_{01}	$1.11 \times 10^{-10}\ \mathrm{mA/cm^2}$
saturation current density (diode 2) J_{02}	$2.28 \times 10^{-5}\ \mathrm{mA/cm^2}$
series resistance R_s	$0.79\ \Omega \cdot \mathrm{cm^2}$
shunt resistance R_{sh}	$1.3 \times 10^7\ \Omega \cdot \mathrm{cm^2}$

APPENDIX
MODELING INPUT PARAMETERS

In this Appendix, we provide information about the input parameters used in this work for the analytical and numerical modeling.

A. Analytical Model

To describe the *I–V* characteristics of the subcells used in the analytical model, we use the two-diode model equation [8]

$$J = J_{Ph} - J_{01} e^{\frac{V + J R_s}{V_T}} - J_{02} e^{\frac{V + J R_s}{2V_T}} - \frac{V + J R_s}{R_{sh}} \quad (3)$$

where J is the current density of the cell operated at voltage V. V_T is the thermal voltage at 25 °C. The remaining input parameters are shown in Table II.

B. Numerical Model

For the numerical modeling in this work, we use the solar cell simulator Griddler [7]. The cell and contacting geometry

TABLE III
GRIDDLER INPUT PARAMETERS FOR THE NUMERICAL MODELING

input parameter	input value
finger sheet res	25.95 $m\Omega/sq$
busbar sheet res	varied
finger contact res	5 $m\Omega \cdot cm^2$
layer sheet res	100 Ω/sq
wafer internal series resistance	26 $m\Omega \cdot cm^2$
contact points resistance	varied
1-sun JL, nonshaded area	41.57 mA/cm^2
front passivated area J01	79 fA/cm^2
front metal contact J01	183 fA/cm^2
rear metal contact J01	70 fA/cm^2
front illumination	1 sun

Parameters not listed are set to 0. For the rear side full area chuck contacting is used.

are imported using *.dxf files. The BB sheet resistance and the contact points resistance are varied for the corresponding parts of this work. The remaining input parameters are shown in Table III.

ACKNOWLEDGMENT

C. Kruse would like to thank J. Wong of the Solar Energy Research Institute of Singapore for his help concerning Griddler simulations.

REFERENCES

[1] B. Hund *et al.*, "Possible impact of systematic errors in IV-measurement," in *Proc. 23rd Eur. Photovoltaic Sol. Energy Conf. Exhib.*, Valencia, Spain, 2008, pp. 1682–1686.

[2] Y. Hishikawa, H. Tobita, A. Sasaki, and Y. Tsuno, "Effects of the distribution of electric potential on the I-V measurement of crystalline silicon Bare Cells," in *Proc. 25th Eur. Photovoltaic Sol. Energy Conf. Exhib./5th World Conf. Photovoltaic Energy Convers.*, Valencia, Spain, 2010, pp. 2663–2666.

[3] I. Geisemeyer, C. Kallies, J. Hohl-Ebinger, and W. Warta, "Contacting bare silicon solar cells with advanced cell metallisation," in *Proc. 29th Eur. Photovoltaic Sol. Energy Conf. Exhib.*, Amsterdam, The Netherlands, 2014, pp. 1202–1207.

[4] R. A. Sinton, "Characterization issues for bifacial solar cells," presented at the bifi PV Workshop, Konstanz, Germany, 2012.

[5] K. A. Emery, "How [NOT] to measure a solar cell to get the highest efficiency," presented at the 43rd IEEE Photovoltaic Spec. Conf., Portland, OR, USA, 2016.

[6] J. Hohl-Ebinger, D. Grote, B. Hund, A. Mette, and W. Warta, "Contacting bare solar cells for STC measurements," in *Proc. 23rd Eur. Photovoltaic Sol. Energy Conf. Exhib.*, Valencia, Spain, Sep. 2008, pp. 2012–2016.

[7] J. Wong, "Griddler: Intelligent computer aided design of complex solar cell metallization patterns," *Proc. IEEE Photovoltaic Spec. Conf.*, 2013, pp. 933–938.

[8] C. Sah, R. Noyce, and W. Shockley, "Carrier generation and recombination in P-N junctions and P-N junction characteristics," *Proc. IRE*, vol. 45, no. 9, pp. 1228–1243, Sep. 1957. [Online]. Available: http://ieeexplore.ieee.org/document/4056679/

[9] B. Lim, T. Brendemuhl, T. Dullweber, and R. Brendel, "Loss analysis of n-type passivated emitter rear totally diffused back-junction silicon solar cells with efficiencies up to 21.2%," *IEEE J. Photovoltaics*, vol. 6, no. 2, pp. 447–453, Mar. 2016. [Online]. Available: http://ieeexplore.ieee.org/lpdocs/epic03/wrapper.htm?arnumber=7400919

[10] pv-tools GmbH, D-88289 Waldburg, Germany. [Online]. Available: www.pv-tools.de

[11] W. Wöger, "Remarks on the En-criterion used in measurement comparisons," *PTB-Mitteilungen*, vol. 109, no. 1, pp. 19–27, 1999.

Authors' photographs and biographies not available at the time of publication.